

Design Principles and Guidelines for Phased Array and Reflector Antennas

Sudhakar K. Rao and Calen Ostroot

Phased array (PA) and reflector antennas are widely used in spacecraft, aircraft, and ground communications applications. This article provides design equations and guidelines that engineering professionals can use for the quick and reasonably accurate design of these antennas without resorting to time-consuming simulations. It also provides insight into the various parameters and their impact on radio-frequency (RF) performance and antenna designs.

INTRODUCTION

Antenna systems used for satellite communications, ground terminals, aircraft applications, and deep-space and wireless communications are getting more complex due to stringent requirements imposed on the industry. These include improved efficiency, low cross-polarization (X-pol), wider coverage, large beam scan, and low front-end losses. PA antennas and reflector antennas are widely used for these applications [1], [2]. Engineering professionals often spend a significant amount of time performing design tradeoffs and RF simulations before arriving at optimal solutions. This could take sev-

EDITOR'S NOTE

Phased array and reflector antennas are widely used in satellite, aircraft, radar, and ground communications. The design of these complex antenna systems is very time consuming since various antenna configurations must be traded off before finalizing the antenna design, which could take several months. In this issue's "Antenna Applications Corner" column, Calen Ostroot and I describe a systematic design approach to finalize the antenna designs for any given requirements within a few days instead of a few months without resorting to detailed analysis and trades. Design guidelines and equations that are useful to engineering professionals are provided in this article, including insight of various parameters and their impact on the radio-frequency (RF) performance. Useful parametric design curves are presented and discussed. An antenna engineer should be able to complete the majority of the antenna aperture design without resorting to tedious RF simulations using the approach presented in this article.



Sudhakar K. Rao

eral months, and, often, such tasks need to be completed within a short period of time, especially for business-development proposals. Figure 1 shows the deployed view of an advanced extremely high frequency (AEHF) satellite, which has three PAs and 10 different reflector antennas for cross-link, downlink, and uplink communications.

This article presents design principles, equations, and guidelines useful for practicing engineers and researchers for reasonably accurate design of these antenna systems within few hours once

the antenna system requirements are given. Various parameters that need to be considered in the design of these antennas are addressed, including their impact on RF performance. The antenna design is simple as long as all of the relevant parameters are properly considered. Parametric design curves are generated for systematic design and performance evaluation of PAs and reflector antennas. Once the antenna system is selected, detailed evaluation and simulations can be carried out at a later stage before the antenna configuration is finalized.

PA ANTENNAS

PA antennas are often used for applications requiring reconfigurable beams. Beam reconfiguration includes beam scanning capability over a certain coverage region, change of beam shape electronically, and mitigation of interferers by creating nulls in the direction of interferers. They can also be used to produce a single transmit (Tx)/receive (Rx) beam over a wide scan range of approximately $\pm 70^\circ$ using transmit/receive modules for radar applications or to generate single/multiple beams for geostationary satellite applications, for which each beam must be scanned independently over a global field of view of $\pm 8.7^\circ$. A typical block diagram of a Rx PA for satellite applications is shown in Figure 2. Multiple beams are generated using low-level [after low-noise amplifiers (LNAs)] beamforming networks, variable phase shifters, and variable attenuators to minimize impact on the gain-to-noise/temperature ratio (G/T).

System and antenna requirements typically are scan coverage, beam diameter, effective isotropic radiated power, G/T , polarization, sidelobe levels, X-pol levels, operational frequency band, and bandwidth. Antenna design parameters to meet these requirements must be selected properly, and they typically include array lattice, interelement spacing or element size, number of elements of the array, and type of radiating element.

ARRAY LATTICE AND GRATING LOBES

The array layout for regular periodic arrays employs either square or hexagonal lattice. The latter is generally preferred for moderate to small scan angles, such as with geostationary communication satellites, due to the reduced number of elements. Square lattice is typically used for wide-beam scan applications, such as radars, due to lower scan loss. The two lattice geometries are shown in Figure 3. For practical designs, arrays must be designed with grating lobes that are placed just outside the coverage region to reduce the element count and complexity of the array. Element spacing



FIGURE 1. An AEHF satellite with multiple PAs and reflector antennas. The inset shows various antennas deployed. (Source: Northrop Grumman Aerospace Systems; used with permission.)

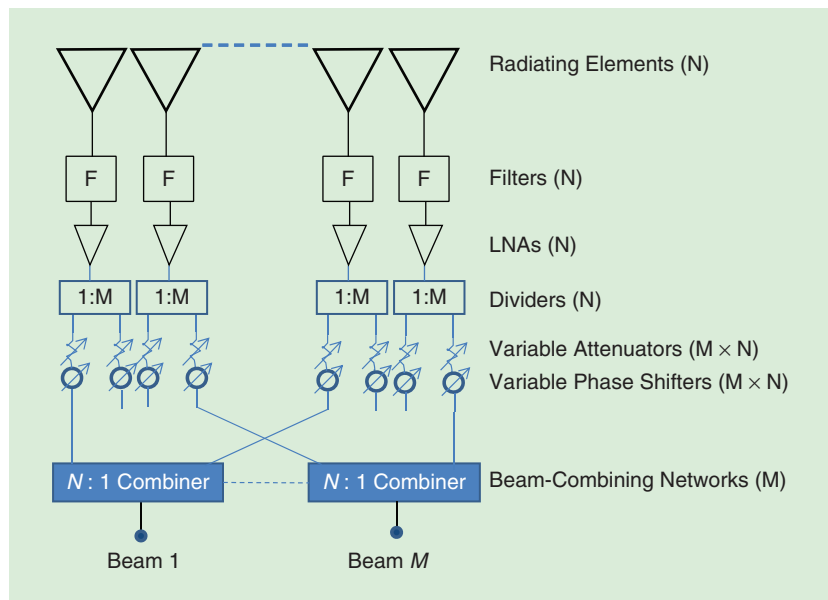


FIGURE 2. A typical block diagram of a PA antenna for multiple-beam applications.

can be determined using the following equations [2]:

$$\frac{d_s}{\lambda_h} \leq \frac{1}{\sin \theta_{sm} + \sin \theta_G}, \quad (1)$$

$$\frac{d_h}{\lambda_h} \leq \frac{1.1547}{\sin \theta_{sm} + \sin \theta_G}, \quad (2)$$

where d_s and d_h are the interelement spacings for the square and hexagonal lattices, θ_{sm} is the maximum coverage/scan

angle from the antenna boresight, θ_G is the location of the closest grating lobe, and λ_h is the wavelength at the highest frequency of operation.

For the square lattice, the closest grating lobes occur in the $\phi = 0^\circ$ and 90° planes. The worst-case grating lobes for the hexagonal lattice array occur in the $\phi = 30^\circ$ and $\phi = 90^\circ$ planes, as illustrated in Figure 3(b).

The grating lobes occur in the opposite direction of the beam scan. The worst-case grating lobe location θ_G is typically selected such that it is larger than θ_{sm} to keep the grating lobe roll-off at least 15 dB lower than the peak gain at the edge of the coverage region. For radar applications where the grating lobes are not desired in the visible space, θ_G will be 90° , and (1) becomes that shown in [3] for this special case. Even for such cases, θ_G could be less than 90° but just outside the scan coverage to increase the element spacing and reduce the number of elements.

Table 1 shows the element spacing required for both lattices as a function of maximum scan angle. The grating lobe location is assumed to be slightly larger than the maximum scan angle and could be changed based on the requirements. It shows that for satellite applications, large element spacing of up to 3.6λ could be used with

Antenna designers should pay attention to scan blindness phenomenon, where the array does not radiate the RF energy but totally reflects the RF signals at certain angles.

hexagonal lattices, whereas for aircraft and radar applications requiring approximately 60° scan, small element spacing of about 0.56λ can be used for arrays with square lattices. Antenna designers should pay attention to scan blindness phenomenon, where the array does not radiate the RF energy but totally reflects the RF signals at certain angles. This is typically the case for wide scan arrays, and the element and array must be designed to avoid scan blindness with such methods as creating a cavity

around each unit cell by using via-holes or optimizing element design over the scan region, among others.

NUMBER OF ELEMENTS AND SCAN LOSS

Once the array lattice and interelement spacing are selected, the number of elements and element type can be determined based on the minimum gain required over the coverage region.

The array peak directivity (D_p) at boresight is given as [4]

$$D_p = 10 \log_{10}(N) + 10 \log_{10} \left[\eta_e \frac{4\pi A_e}{\lambda_l^2} \right], \quad (3)$$

where D_p is in dBi and is the product of the element directivity and the number of elements in the array; A_e is the unit-cell area of the element, λ_l is the wavelength at the lowest frequency of operation, η_e is the element efficiency, and N is the number of elements in the array. The first term on the right-hand side of (3) is the array factor, and the second term is the element directivity D_e . The number of elements for the array can be calculated as

$$N = 10^{(0.1D_p - 0.1D_e)}. \quad (4)$$

The peak directivity can be derived from the minimum gain requirement over the coverage region and is given as

$$D_p = G_{min} + L_s + SL + GL_{pe} + T_L + X + I_m, \quad (5)$$

where G_{min} is the minimum gain of the array over the coverage, L_s is the antenna loss that includes all front-end losses (from array aperture to amplifiers, including mismatch loss, polarization loss, insertion loss, and so on), SL is the scan loss, GL_{pe} is the gain loss due to pointing error (satellite, aircraft, or ground pointing error), T_L is the illumination taper loss of the array in dB, X is the loss over the beam diameter (3 dB typically, 0 dB if only the beam peak is the requirement), and I_m is the implementation margin. I_m is required for practical array antennas to account for thermal effects, loss due to

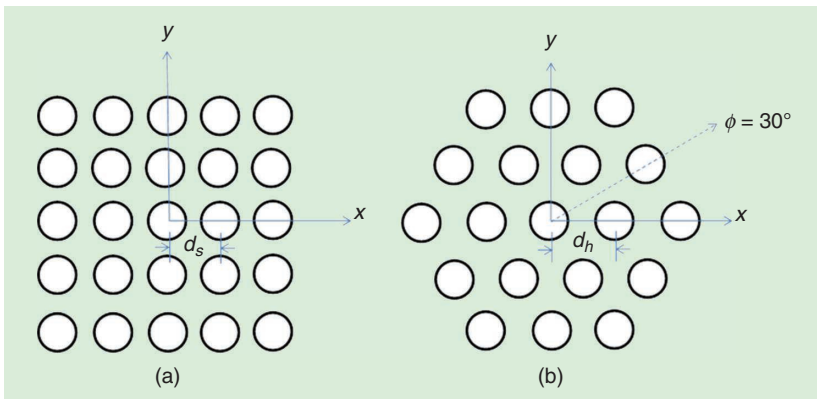


FIGURE 3. The array layouts of elements using (a) a square grid and (b) a hexagonal grid.

TABLE 1. THE ELEMENT SPACING FOR SQUARE AND HEXAGONAL LATTICES AS A FUNCTION OF MAXIMUM SCAN ANGLE.

θ_{sm} ($^\circ$)	θ_G ($^\circ$)	d_s/λ	d_h/λ
5	6	5.22	6.02
8.7	9.7	3.13	3.61
15	16	1.87	2.16
30	32	0.97	1.12
45	47	0.7	0.8
60	65	0.56	0.66
70	75	0.52	0.61
80	85	0.5	0.58

thermal blanket covering the array, gain degradation due to amplifier failures, and array excitation amplitude and phase errors (typically, 0.5–1 dB). The scan loss depends only on the element size and is given by the element gain roll-off from beam peak to the maximum scan angle. The element roll-off for directive elements ($>1\lambda$, typically used for satellites with small coverage regions or scans) is given as

$$SL = 3\left(\frac{\theta_{sm}}{0.5\theta_3}\right)^2, \quad (6)$$

where θ_{sm} is the maximum scan angle over the coverage, and θ_3 is the half-power beamwidth of the radiating element, which depends on the type of radiating elements and is given by

$$\theta_3 = A(\lambda_h/d_e). \quad (7)$$

In (7), d_e is the element diameter, and A is a constant that depends on the type of radiating element. A is 63 for a high-efficiency multimode horn, 70 for a Potter horn, 75 for a corrugated horn, 58 for a cup-dipole radiating element, 55 for a dominant-mode square horn, and 52 for a high-efficiency square or rectangular horn. The scan loss for element sizes close to 0.5λ used for large scan applications is given as

$$SL = 10 \log_{10}(\cos^n \theta). \quad (8)$$

The value of n varies and is typically in the range of 1–1.5. For small elements, a value of $n = 1.5$ in (8) better fits the element roll-off than the conventional $\cos(\theta)$ roll-off for practical antennas. For example, the scan loss is 2.26 dB for a 45° scan, 4.52 dB for a 60° scan, and 6.99 dB for a 70° scan.

AMPLITUDE TAPER

The array amplitude taper is one of the critical parameters impacting the gain and sidelobe levels. The arrays are uniformly illuminated if low sidelobes are not required. This is due the facts that the beamforming network is simpler and, also, all of the distributed amplifiers for Tx arrays could have uniformly sized solid-state power amplifiers. A tapered illumination distribution lowers the sidelobe

The array amplitude taper is one of the critical parameters impacting the gain and sidelobe levels.

levels but broadens the beam and lowers the antenna efficiency. A parabolic aperture distribution over a pedestal maximizes the antenna efficiency for a given sidelobe level and is often used in practical arrays instead of Gaussian-type distribution. The aperture-field-illumination function is defined as

$$E(r) = T + (1 - T)(1 - r^2)^n, \quad (9)$$

where r is the normalized radius, T is the pedestal height at the edge of the array, and n is the shape factor. Edge illumination taper in decibels is given as $20 \log_{10}(T)$. A higher value for the shape factor gives lower efficiency. A shape factor of $n = 1$ is generally used in practice. The efficiency value for $n = 1$ as a function of pedestal height T is given in closed form as

$$\eta = 75 \frac{(1 + T)^2}{(1 + T + T^2)}. \quad (10)$$

The efficiency value η in (10) is a percentage. For example, a 5-dB edge taper gives an efficiency value of 97.4%, and a 10-dB illumination taper ($T = 0.316$)

provides an aperture efficiency of 91.7%. Gain loss due to a 10-dB taper is only 0.38 dB. This must be taken into account in array sizing.

The analysis provided here is intended for quick design and performance-evaluation purposes only. Once the design is completed, detailed performance is necessary, including finite array effects, which are critical for smaller arrays, and mutual coupling effects, which are more critical for wide-scan applications due to smaller element sizes. However, for geostationary satellites, the element sizes are approximately 3λ , and mutual coupling is negligibly small.

DESIGN EXAMPLE

A 169-element array with 3λ interelement spacing is used in this example. The elements are arranged in a hexagonal-grid layout and fit close to a circular aperture diameter of 40λ , as shown in Figure 4. Computed array patterns for boresight and scanned beams are shown in Figures 5 and 6, respectively. The directivity plot of the boresight beam as a function of θ is shown in Figure 5. The nearest grating lobe is at -22.5° . The grating lobe plot for the beam scanned to 9° and the corresponding directivity plot are shown in Figure 6. The scanned beam nearest the grating lobe is at -13.5° relative to boresight direction.

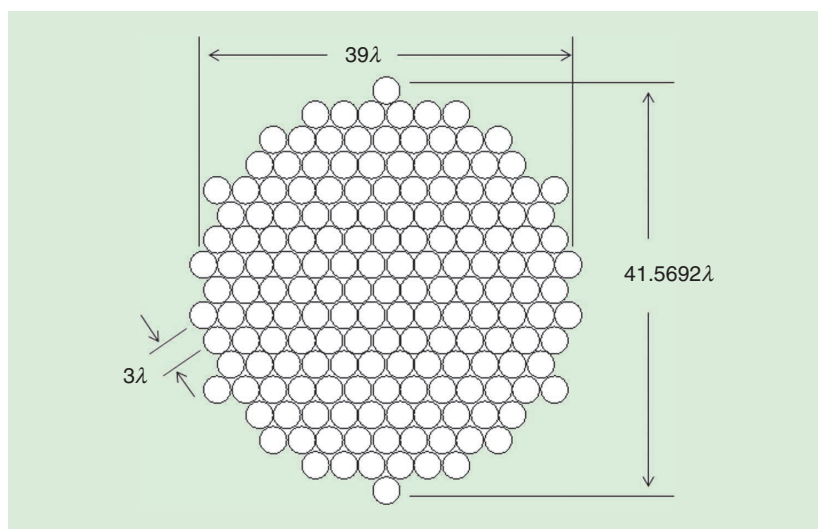


FIGURE 4. The planar array geometry with 169 elements arranged in a hexagonal lattice.

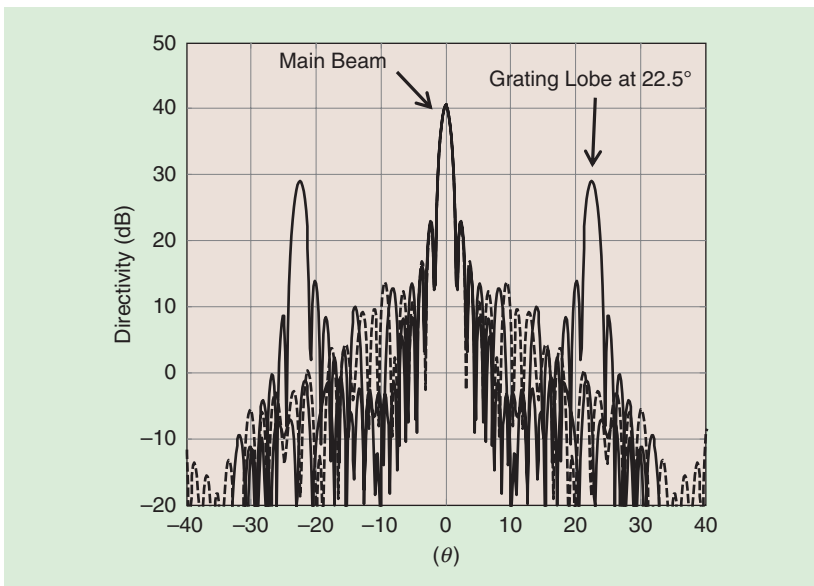


FIGURE 5. Computed directivity patterns of the boresight beam for the array geometry in Figure 4. The closest grating lobes are at $\pm 22.5^\circ$.

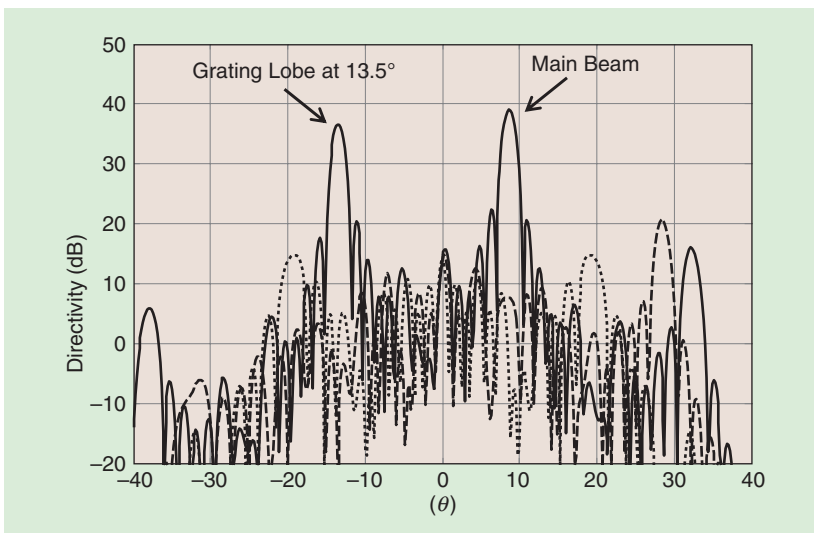


FIGURE 6. The computed directivity patterns of the scanned beam for the array geometry in Figure 4. The closest grating lobe is at -13.5° .

PARAMETRIC DESIGN CURVES

Design curves that are useful for antenna engineers are discussed here. Figure 7 shows the plot of antenna directivity and grating-lobe locations as a function of element spacing normalized to wavelength. Parameters of the curves are the boresight beam and scanned beam to 8.7° (representing the edge of Earth from a geostationary satellite). The arrays are assumed to be designed in a hexagonal lattice with the number of elements constant at 469. For a 3.5λ spacing, the peak and edge-of-coverage

directivity values are 47.2 and 44.1 dBi, respectively.

The worst-case scan loss over the coverage is 3.1 dB, which is due to element pattern roll-off associated with the 3.5λ horn. The worst-case grating lobe locations are 19.5° and 10.5° for the boresight and edge-scanned beams, respectively. The PA should be designed with grating lobes (as long as they appear outside the coverage region) to minimize the number of elements for a given directivity to reduce the array complexity and cost. Since the directivity depends on

the number of elements (array factor) and the element directivity, the element design must be optimized to achieve maximum efficiency.

With element spacing fixed as 3.5λ , the number of elements is varied, and the directivity plots are shown in Figure 8 for boresight and scanned beams. The difference between the blue and red curves is the scan loss, which is constant, derived from the 3.5λ horn pattern roll-off at 8.7° . The parametric curves shown in Figures 7 and 8 are useful for quick design of PA antennas.

RADIATING ELEMENTS

It is necessary to choose the optimum radiating elements for PAs based on the bandwidth, polarization, and, more importantly, efficiency. For satellite applications with a limited coverage region of $\pm 8.7^\circ$, element spacing in the range of $3\lambda - 3.5\lambda$ is preferred, as discussed previously. This is due to the need to minimize the number of elements and reduce the complexity of PAs. Smooth-walled horns are preferred for these applications instead of corrugated horns [5], [6] to achieve better efficiency. Corrugated horns have thick walls due to corrugations and are not suitable for array applications. Potter horns and multimode horns are suitable, where 70% efficiency can be achieved with Potter horns (using TE₁₁ and TM₁₁ modes) [7], and approximately 85–90% efficiency can be achieved using multimode, multiflare, high-efficiency horns using TE₁₁ and TE_{1n} modes [8], [9].

A comparison of radiating elements for the three types is given in Table 2 for 3.5λ -diameter horns. The results are based on computed patterns of the optimized geometries of the three types of horns and some measured data. Corrugated horns with hybrid HE₁₁ mode propagation have low element efficiency because the electrical aperture is smaller than the physical aperture due to thick corrugations. Dual-mode Potter horns provide efficiency values of approximately 70% and have limited bandwidth; they also are not preferred. Multimode, multiflare horns are preferred for array applications due to

high efficiency values of approximately 85–93% and lighter weight compared to corrugated horns. Multimode horns with slope discontinuities can cover multiple frequency bands and could be used for dual-band and tri-band applications as well [10], [11].

REFLECTOR ANTENNAS

There are several types of reflector antennas, including single reflector and dual reflector, that operate in center-fed or offset-fed configurations [12]. However, offset-fed single reflectors are preferred and often used in the satellite industry due to avoidance of blockage effects, ease of packaging on the spacecraft structure, and convenient location of the feed with minimal loss. Offset reflectors do not depolarize signals for circular polarization but cause beam squint [13], [14]. The feed polarization must be opposite to the sense of the desired circular polarization since the polarization sense changes after reflection from the surface of the reflector. (For dual-reflector antennas, the feed polarization is the same as that of the desired circular polarization.)

Offset single reflectors create X-pol for linear polarizations, which can be minimized by choosing the geometrical parameters appropriately. The feed phase center is typically placed at the focal point of the reflector. The phase center of the feed varies with frequency, and the phase center at the center of the frequency band can be placed at the focal point of the reflector to optimize the reflector-antenna performance over the desired bandwidth [15]. For Rx antennas, the system noise temperature is important to achieve better G/T of the antennas; passive intermodulation should be considered carefully for a multicarrier Tx/Rx antenna system in the design, manufacture, and qualification of these antennas for space applications.

This section deals with single reflectors that operate in the offset configuration, but details for the other reflector types are given in [12]. Figure 9 shows the offset reflector geometry with critical parameters, such as diameter of the reflector (projected aperture diameter D), focal length (F), and offset clearance height (h). The offset height must be selected based on avoiding geometrical

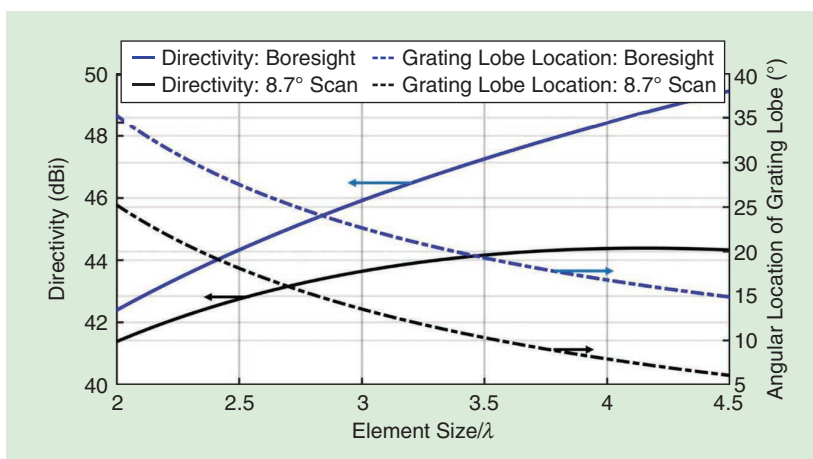


FIGURE 7. The parametric design curves of a PA with hexagonal lattice. Parameters are directivity and grating lobe locations as a function of element spacing ($N = 469$).

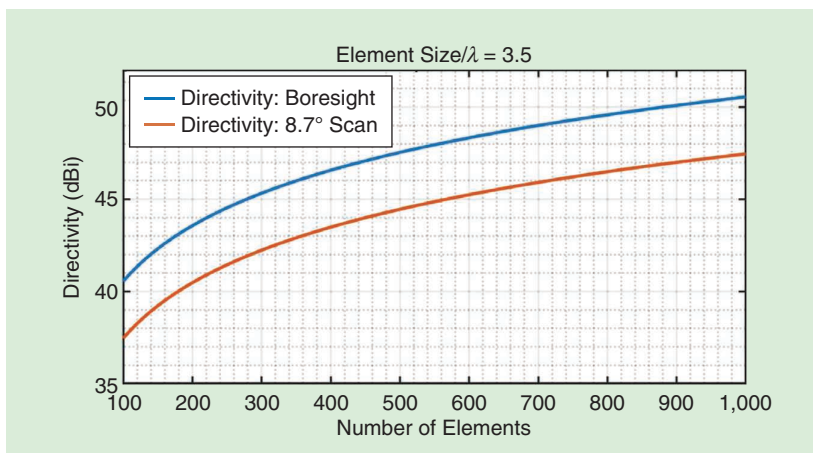


FIGURE 8. The parametric design curves of a PA with hexagonal lattice showing variation of directivity with number of elements. The element spacing is constant at 3.5λ .

TABLE 2. A COMPARISON OF RADIATING ELEMENTS FOR 3.5λ HORNS.

	Corrugated Horn	Dual-Mode Potter Horn	High-Efficiency Horn
K_a band	30–31	30–31	30–31
EHF band	43.5–45.5	43.5–45.5	43.5–45.5
Polarization	RHCP	RHCP	RHCP
Return loss K_a (dB)	28	29	30
Return loss EHF (dB)	25	N/A	31
Efficiency at K_a (%)	58	70	91
Efficiency at EHF (%)	54	N/A	85
X-pol K_a (dB)	–35	–32	–31
X-pol EHF (dB)	–31	N/A	–33

RHCP: right-hand circularly polarized; N/A: not applicable.

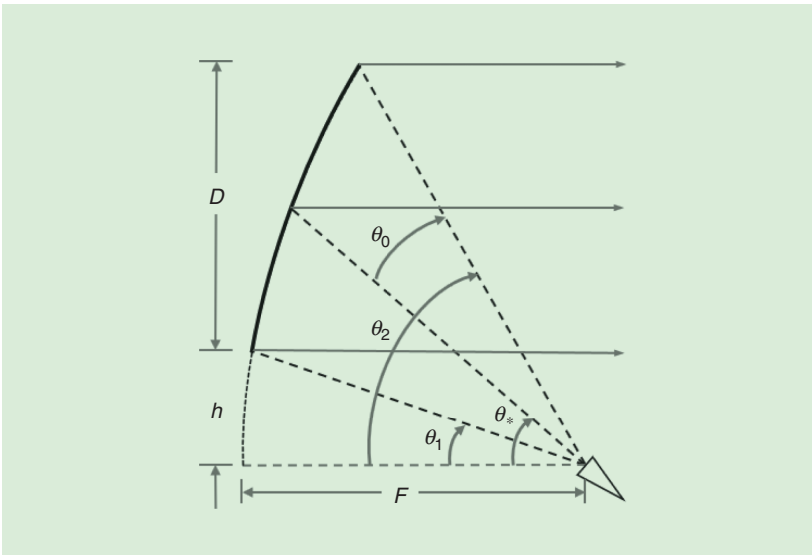


FIGURE 9. The geometry of an offset reflector antenna.

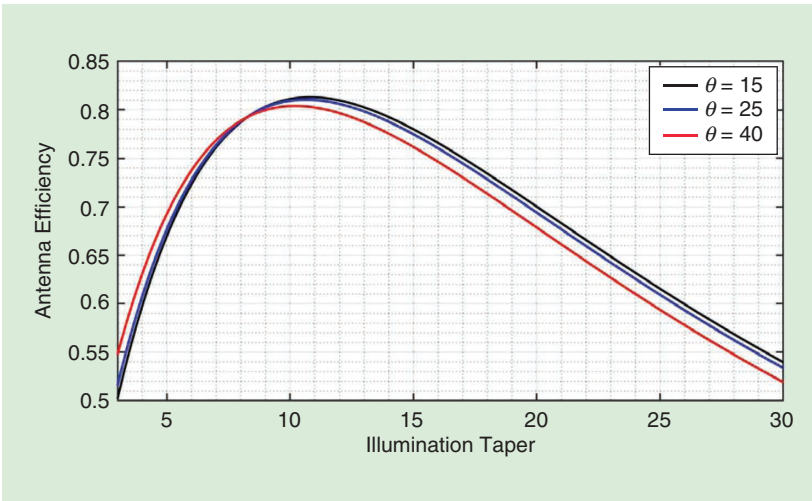


FIGURE 10. Reflector antenna efficiency as a function of illumination taper.

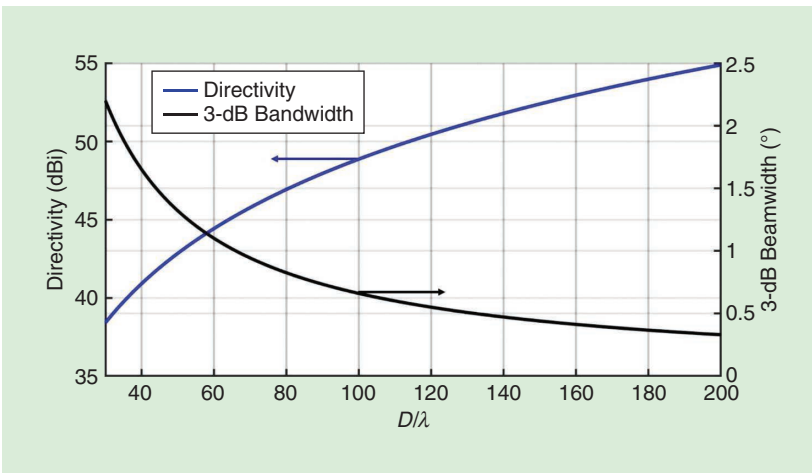


FIGURE 11. Reflector antenna directivity and half-power beamwidth as a function of reflector diameter (D/λ).

blockage over the desired coverage region while keeping it as small as possible. F/D is typically in the range 0.6–1.5, depending on the application. For multiple beam applications, a large F/D in the range of 1–1.5 is desired to minimize the scan loss over the desired coverage. The feed is placed such that the phase center is at the focal point of the reflector. The angular parameters in Figure 9 are given for an offset parabolic reflector as

$$\theta_{*,0} = \frac{1}{2} \left(\tan^{-1} \left[\frac{D+h}{F - \frac{(D+h)^2}{4F}} \right] \pm \tan^{-1} \left[\frac{h}{F - \frac{h^2}{4F}} \right] \right), \quad (11)$$

$$\theta_2 = (2\theta_0 + \theta_1), \quad (12)$$

$$\theta_1 = \theta_* - \theta_0, \quad (13)$$

where θ_* is the feed-tilt angle from the focal point to vertex of the reflector to the center of the reflector aperture so that the feed has maximum illumination at the center of the reflector and provides the required taper at the reflector edges.

The illumination taper on the reflector is dictated by the angle θ_0 and the feed size. The antenna directivity depends on the aperture diameter D and efficiency η_f and is given as

$$D = 10 \log_{10} \left[\frac{4\pi A}{\lambda^2} \eta_f \right], \quad (14)$$

$$\eta_f = 4 \cot^2 \left(\frac{\theta_0}{2} \right) \left[1 - \cos^n \left(\frac{\theta_0}{2} \right) \right]^2 \frac{(n+1)}{n^2}. \quad (15)$$

In (14), A is the aperture area of the reflector, and λ is the wavelength. The value of n depends on the illumination taper T on the reflector and is related as

$$n = \frac{-0.05T}{\log_{10} \left[\cos \left(\frac{\theta_0}{2} \right) \right]}. \quad (16)$$

The feed horn field illumination is assumed as $\cos^n(\theta/2)$ angular variation in (15). T is the illumination taper in positive decibels. Most of the horn patterns can be modeled with this assumption for the main beam. Aperture efficiency η_f is plotted as a function of the feed illumination taper on the reflector edge (T) in Figure 10. The variable in the curves is the angle θ_0 . The optimum illumination

taper is in the range of 10–12 dB. Larger tapers will reduce the illumination efficiency, and smaller tapers will reduce the spill-over efficiency.

The next parameter of interest is the half-power beamwidth. This is related to illumination taper T and is given as [12]

$$\theta_3 = (0.762T + 58.44) \frac{\lambda}{D}. \quad (17)$$

For certain applications, the beam must be scanned away from the antenna boresight. This is achieved by moving the feed horn from the focal point and placing it appropriately in the focal plane. For a given scan angle of θ_s , the feed displacement in the focal plane is given as

$$\theta_s = d_s S_F, \quad (18)$$

where S_F is the scan factor, which is defined as the ratio of the electrical scan angle of the beam to the displacement of the feed horn in the focal plane from the focal point; it has units of degrees per inch. The scan factor depends on the reflector geometry and can be calculated easily, as reported previously [16], [17]

$$S_F = \frac{1 + x \left(\frac{D}{4F} \right)^2}{1 + \left(\frac{D}{4F} \right)^2} \left\{ \frac{1 + \cos \theta_2}{2F} \right\} \left(\frac{180}{\pi} \right). \quad (19)$$

The scanned beams suffer from gain loss from the unscanned beam, and the gain loss GL (in decibels) is given as [17]

$$GL = \frac{0.0015\delta^2}{\left[\left(\frac{F}{D_p} \right)^2 + 0.02 \right]^2 + \frac{0.011\delta}{\left[\left(\frac{F}{D_p} \right)^2 + 0.02 \right]}}, \quad (20)$$

where δ is the number of beamwidths (half power) scanned from the antenna boresight, and D_p is the diameter of the parent paraboloid [$D_p = 2(D + h)$]. The beamwidth broadens as the beam is scanned, and the scanned-beam half-power beamwidth is given as

$$\theta_3(\delta) = \theta_3(\delta = 0) 10^{0.05GL}. \quad (21)$$

These equations provide a simple design methodology and quick performance evaluation for reflector antennas. Antenna directivity and half-power beamwidths

are plotted in Figure 11 as a function of reflector aperture diameter D/λ . The antenna efficiency of 78%, corresponding to illumination taper $T = 10$ dB, is assumed in the plot.

There is also another class of antennas, not considered here, that is widely used in satellite communications and employs PA-fed reflectors to generate multiple beams or area beams for mobile communications and other applications. These systems use a small PA and a large reflector (either single-piece or deployed-mesh reflectors) and are called *imaging reflector antennas* since the feed array is defocused from the focal plane to create imaging optics [12].

SUMMARY AND CONCLUSIONS

A systematic design and performance analysis were presented for PA and offset-single-reflector antennas. This enables engineers to perform quick designs and evaluations within a few hours without resorting to time-consuming analysis with commercial software codes. This article can be useful when performing antenna trades to select the optimal antenna configuration for given RF requirements.

ACKNOWLEDGMENT

This work was supported by Northrop Grumman Aerospace Systems Internal Research and Development.

AUTHOR INFORMATION

Sudhakar K. Rao (sudhakar.rao@ngc.com) is a technical fellow at Northrop Grumman Aerospace Systems, Redondo Beach, California, working on antenna systems for satellites, aircraft, and ground applications. He is the recipient of the 2009 IEEE Judith Resnik Technical Field Award for pioneering work in aerospace engineering. He is a Life Fellow of the IEEE.

Calen Oostroot (Calendavid13@gmail.com) is a fourth-year electrical engineering major at the University of California, Los Angeles, where he is the vice president of the Super-Mileage Vehicle Team and an intern at Northrop Grumman Aerospace Systems. His research interests include various types of antennas, including lenses, digital phased arrays, reflector

antennas, multiband patch antennas, and additive manufacturing.

REFERENCES

- [1] S. Rao, "Advanced antenna technologies for satellite communications payloads," *IEEE Trans. Antennas Propag.*, vol. 63, no. 4, pp. 1205–1217, Apr. 2015. doi: 10.1109/TAP.2015.2391283.
- [2] S. Rao, M. Tang, and C.-C. Hsu, "Multiple beam technologies for satellite communications payloads," *Appl. Comput. Electromagn. Soc. J.*, vol. 21, no. 3, pp. 353–364, Nov. 2006.
- [3] R. J. Mailloux, *Phased Array Antenna Handbook*. Norwood, MA: Artech House, 1994, ch. 1, p. 31.
- [4] S. Rao, F. Mayol, M. Padilla, R. Sudarsanam, and S. Chun, "Array antennas and low-gain TT&C antennas," in *Handbook of Reflector Antennas & Feed Systems*, vol. 2, L. Shafai, S. Sharma and S. Rao, Eds. Norwood, MA: Artech House, 2013, ch. 9, pp. 299–349.
- [5] G. L. James, "Design of wide-band corrugated horns," *IEEE Trans. Antennas Propag.*, vol. 32, no. 10, pp. 1134–1138, Oct. 1984. doi: 10.1109/TAP.1984.1143203.
- [6] S. Rao, "A simple dual-band corrugated horn with low cross polarization," *IEEE Trans. Antennas Propag.*, vol. 38, no. 6, pp. 946–951, June 1990. doi: 10.1109/8.55598.
- [7] P. D. Potter, "A new horn antenna with suppressed sidelobes and equal beamwidths," *Microw. J.*, vol. 6, no. 6, pp. 71–78, 1963.
- [8] K. K. Chan and S. Rao, "Design of high efficiency circular horn feeds for multi-beam reflector antennas," *IEEE Trans. Antennas Propag.*, vol. 56, no. 1, pp. 253–258, Jan. 2008. doi: 10.1109/TAP.2007.913172.
- [9] S. Rao and M. Tang, "High-efficiency horn for an antenna system," U.S. Patent 7 463 207, Dec. 9, 2008.
- [10] S. Rao, C.-C. Hsu, and K. K. Chan, "Antenna system supporting multiple frequency bands and multiple beams," *IEEE Trans. Antennas Propag.*, vol. 56, no. 10, pp. 3327–3329, Oct. 2008. doi: 10.1109/TAP.2008.929540.
- [11] S. Rao, C.-C. Hsu, and G. Matyas, "Dual-band antenna using high/low efficiency feed horn for optimal radiation patterns," U.S. Patent 8 514 140, Aug. 20, 2013.
- [12] C. Babu Ravipati and S. Rao, "Advanced reflector antennas," in *Handbook of Reflector Antennas and Feed Systems*, vol. 1, S. Sharma, S. Rao, and L. Shafai, Eds. Boston: Artech House, 2013, ch. 7, pp. 219–246.
- [13] T. S. Chu and R. H. Turrin, "Depolarization properties of offset reflector antennas," *IEEE Trans. Antennas Propag.*, vol. 21, no. 3, pp. 339–345, May 1973. doi: 10.1109/TAP.1973.1140479.
- [14] N. A. Adatia and A. W. Rudge, "Beam-squint in circularly-polarized offset reflector antennas," *Electron. Lett.*, vol. 11, no. 21, pp. 513–515, Oct. 1975. doi: 10.1049/el:19750396.
- [15] S. Rao and L. Shafai, "Phase center calculation of reflector antenna feeds," *IEEE Trans. Antennas Propag.*, vol. 32, no. 7, pp. 740–742, July 1984. doi: 10.1109/TAP.1984.1143406.
- [16] S. Rao, "Design and analysis of multiple-beam reflector antennas," *IEEE Antennas Propag. Mag.*, vol. 41, no. 4, pp. 53–59, Aug. 1999. doi: 10.1109/74.789737.
- [17] S. Rao, "Parametric design and analysis of multiple beam reflector antennas for satellite communications," *IEEE Antennas Propag. Mag.*, vol. 45, no. 4, pp. 26–34, Aug. 2003. doi: 10.1109/MAP.2003.1241308.